ARTICLE OPEN

Check for updates

Cereblon (CRBN) inhibits prostate cancer metastasis by negatively regulating 6-phosphogluconate dehydrogenase (6PGD)

Koushik Guchhait[1,11], Hyeon-Seung Yoon[1,11], Hyun-Su An[1], Seungheon Shin[2], Hye Seung Nam[1], Francisco D. Yanqui-Rivera[1], Samara M. Oña[3], Miguel Á. Mendez[3,4], Jong Yeon Hwang[5], Daeho Park[1], Chul-Seung Park[1], Jee-Young Han[6], Doo Yong Chung[7], Seokjae Park[8], Eun-Kyoung Kim[8], Su-Geun Yang[9] and Steve K. Cho[1,2,10]✉

Metastasis is the primary cause of mortality in advanced prostate cancer, and the emergence of resistance to androgen receptor (AR)-targeted therapies highlights the urgent need for alternative therapeutic strategies. Metabolic reprogramming has increasingly been recognized as a key driver of metastatic progression. In this study, we uncover a novel tumor-suppressive role for cereblon (CRBN), a substrate receptor of the CRL4^{CRBN} E3 ubiquitin ligase complex, in modulating prostate cancer metastasis through regulation of 6-phosphogluconate dehydrogenase (6PGD), a critical enzyme in the oxidative pentose phosphate pathway (oxPPP). CRBN directly binds a conserved C-terminal α-helix in 6PGD, promoting its polyubiquitination and proteasomal degradation independently of immunomodulatory drugs (IMiDs). Genetic or pharmacological loss of CRBN via CRISPR/Cas9, RNA interference, or PROTAC-mediated degradation stabilized 6PGD and elevated the NADPH/NADP$^+$ ratio. Conversely, re-expression of wild-type CRBN reduced 6PGD levels, restored NADPH/NADP$^+$ ratio, and suppressed cell migration and invasion. Transcriptomic profiling revealed CRBN-induced upregulation of CDH1 and downregulation of the EMT marker MMP1, while CRBN degradation produced the opposite pattern—both effects were reversed by 6PGD inhibition. These regulatory effects were conserved across multiple cancer cell lines and observed in CRBN-deficient mouse tissues. Functional studies using intra-splenic xenograft models further demonstrated that CRBN suppresses metastatic dissemination. Collectively, our findings identify 6PGD as a novel endogenous substrate of CRBN and establish the CRBN–6PGD axis as a critical metabolic checkpoint in prostate cancer metastasis. Therapeutic targeting of this pathway may offer promising strategies for CRBN-deficient or 6PGD-driven cancers.

Oncogene (2026) 45:1234–1246; https://doi.org/10.1038/s41388-026-03717-9

INTRODUCTION

Prostate cancer remains a leading cause of cancer-related mortality among men worldwide, with its lethality primarily driven by metastatic progression—the main contributor to treatment failure and death in advanced-stage disease [1–3]. Metastasis is a complex, multistep process whereby cancer cells detach from the primary tumor, invade surrounding tissues, and disseminate via the bloodstream or lymphatic system to form secondary tumors in distant organs such as the bone, liver, and lungs [4, 5]. Despite advances in androgen receptor (AR)-targeted therapies, resistance to these agents remains a formidable clinical challenge, underscoring the need to identify alternative molecular drivers of metastasis and develop effective strategies to suppress cancer cell dissemination.

Recent studies have identified cereblon (CRBN) as a key regulatory protein in cancer biology. As a substrate receptor of the cullin-RING (CRL4^{CRBN}) E3 ubiquitin ligase complex, CRBN mediates the ubiquitin-dependent degradation of diverse cellular targets involved in transcription, DNA repair, and cell cycle control [6–10]. CRBN is best known as the pharmacological target of immunomodulatory drugs (IMiDs), including thalidomide and its analogs, which exert anti-proliferative, anti-angiogenic, and immunomodulatory effects in multiple myeloma and other hematologic malignancies [11–13]. Notably, diminished CRBN expression has been associated with poor prognosis and enhanced migratory behavior in various cancer types [14–16]. However, the physiologic substrates of CRBN and its mechanistic role in metastasis remain incompletely understood.

[1]Department of Life Sciences, Gwangju Institute of Science and Technology (GIST), Gwangju, Korea. [2]Department of Biomedical Science and Engineering, Gwangju Institute of Science and Technology (GIST), Gwangju, Korea. [3]Instituto de Simulación Computacional (ISC-USFQ), Universidad San Francisco de Quito, Quito, Ecuador. [4]Colegio de Ciencias e Ingenierías, Politécnico, Universidad San Francisco de Quito, Quito, Ecuador. [5]Therapeutics & Biotechnology Division, Korea Research Institute of Chemical Technology (KRICT), Daejeon, Korea. [6]Department of Pathology, Inha University Hospital, Incheon, Korea. [7]Department of Urology, Inha University Hospital, Incheon, Korea. [8]Department of Brain and Cognitive Sciences, Neurometabolomics Research Center, Daegu Gyeongbuk Institute of Science and Technology (DGIST), Daegu, Korea. [9]Department of Biomedical Science, BK21 FOUR program in Biomedical Science and Engineering, Inha University College of Medicine, Incheon, Korea. [10]Integrated Institute of Biomedical Research (IIBR), Gwangju Institute of Science and Technology (GIST), Gwangju, Korea. [11]These authors contributed equally: Koushik Guchhait, Hyeon-Seung Yoon. ✉email: scho@gist.ac.kr

Received: 17 September 2025 Revised: 23 January 2026 Accepted: 18 February 2026
Published online: 9 March 2026

6-Phosphogluconate dehydrogenase (6PGD), an essential enzyme in the oxidative arm of the pentose phosphate pathway (oxPPP), plays a central role in cancer metabolism. 6PGD catalyzes the oxidative decarboxylation of 6-phosphogluconate to ribulose-5-phosphate, generating NADPH—a critical cofactor that supports reductive biosynthesis and antioxidant defense. These metabolic programs are often co-opted by cancer cells to support proliferation, survival, and metastatic progression [17–19]. Aberrant upregulation of 6PGD has been reported in several cancers, including prostate cancer, where it contributes to tumor growth, invasiveness, and therapy resistance through redox and signaling modulation [17–21]. Nevertheless, the regulatory mechanisms governing 6PGD protein turnover remain poorly defined.

In this study, we identify 6PGD as a previously unrecognized endogenous substrate of CRBN. We demonstrate that CRBN binds directly to 6PGD and promotes its polyubiquitination and proteasomal degradation via the $CRL4^{CRBN}$ complex. Mechanistically, CRBN-mediated degradation of 6PGD limits NADPH production and suppresses epithelial–mesenchymal transition (EMT), thereby inhibiting prostate cancer cell migration, invasion, and metastasis. Conversely, CRBN loss—induced either genetically or pharmacologically—results in 6PGD accumulation and increased metastatic potential. These findings uncover a tumor-suppressive function of CRBN *via* 6PGD regulation, establishing the CRBN–6PGD axis as a key metabolic checkpoint in prostate cancer metastasis with broad therapeutic implications.

MATERIALS AND METHODS

Cell lines and cell culture

RWPE-1 (CRL-11609), DU145 (HTB-81), PC3 (CRL-1435), H1299 (CRL-5803), HEK293T (CRL-3216), MEF (SCRC-1008), and U-87 MG (HTB-14) cells were purchased from ATCC (Manassas, VA, USA). The LNCaP cell line was purchased from the Korean Cell Line Bank (KCLB). RWPE-1, DU145, PC3, LNCaP, and H1299 cells were cultured in RPMI medium (Gibco, 11875093, Grand Island, NY, USA), while HEK293T, MEF, and U-87 MG cells were cultured in DMEM (Gibco, LB00102) supplemented with 2 mM glutamine (Gibco, A2916801), 100 IU/mL penicillin, 100 µg/mL streptomycin (Gibco, 15140-122), and 10% heat-inactivated fetal bovine serum (HyClone, SH30071.03HI, Logan, Utah, USA) at 37 °C in a humidified 5% CO_2 incubator. All cell lines were confirmed to be mycoplasma-free.

Antibodies

Primary antibodies against CRBN (HPA045910) were from Sigma-Aldrich (St. Louis, MO, USA). Anti-CRBN (71810S), CDH1 (3195 T), and rabbit IgG (45262S) were from Cell Signaling Technology (Danvers, MA, USA). Anti-6PGD (ab129199), CUL4A (ab92554), and MMP1 (ab137332) were from Abcam (Cambridge, UK). Additional anti-6PGD (NBP1-31589) was from Novus Biologicals (Centennial, CO, USA). Anti-HA (901501) was from BioLegend (San Diego, CA, USA); anti-Myc (05-419) from Millipore (Darmstadt, Germany); anti-DDB1 (A300-462A) from Bethyl Laboratories (Montgomery, TX, USA); and anti–β-Actin (LF-PA0207) and GAPDH (LF-PA0018) from AB Frontier (San Jose, CA, USA). Rabbit IgG (sc-2027) was from Santa Cruz Biotechnology (Dallas, TX, USA). HRP-conjugated secondary antibodies against rabbit and mouse were from Jackson ImmunoResearch (111-035-003, West Grove, PA, USA).

Retrovirus production and packaging

Retrovirus generation and transduction were conducted per protocols from the Stewart laboratory. Briefly, 1 µg of GFP-CRBN plasmid and 1 µg of retroviral packaging plasmids were co-transfected into HEK293FT cells using FuGENE HD (Promega, E2311, Madison, WI, USA) in serum-free DMEM. Viral supernatant was collected and filtered (0.45 µm) to remove cells. Polybrene (10 µg/mL) was added and incubated with target cells for 8 h. GFP-positive infected cells were sorted using FACS.

Co-immunoprecipitation (Co-IP)

HEK293T cells were seeded to 60% confluency and transfected with expression plasmids using FuGENE or Lipofectamine 2000 (Invitrogen, 11668019, Waltham, MA, USA). After 24 h, cells were harvested, washed in ice-cold DPBS (WELGENE, LB00102, Gyeongsan, Korea), and lysed in NP-40 buffer (Elpisbiotech, EBA-1049, Daejeon, Korea) with protease and phosphatase inhibitors (Xpert). Lysates were rotated for 1 h at 4 °C, centrifuged at 12,500 rpm for 20 min, and supernatants incubated with antibodies overnight. Protein complexes were captured with Protein G Sepharose beads (GE Healthcare, 17061801, Chicago, IL, USA), washed four times, and analyzed by Western blot.

Immunoblot analysis

Cells were lysed in NP-40 buffer with protease and phosphatase inhibitors and incubated for 1 h at 4 °C. After centrifugation (12,500 rpm, 20 min), protein concentrations were determined by Bradford assay (Biosesang, B1017, Yongin, Korea). Equal amounts of protein were separated by SDS-PAGE, transferred to nitrocellulose membranes (BioRad, 1620112, Hercules, CA, USA), and probed with primary and HRP-conjugated secondary antibodies. Signals were visualized by ECL detection (GE Healthcare, RPN2109) and film development (Fujifilm, 47410, Tokyo, Japan).

In vivo ubiquitination assay

As previously described [22], cells were transfected with HA-ubiquitin (2 µg) and treated with MG132 (10 µM) or MLN4924 (25 µM) for 4 h. Cells were lysed in 200 µL of NP-40 buffer containing 1% SDS and boiled at 100 °C for 5 min. IP buffer (800 µL) was added, immunoprecipitations were performed, and analyzed by immunoblotting.

RNA isolation and qRT-PCR

Total RNA was extracted using TRIzol (Ambion, 1596026, Austin, TX, USA) and purified with the Direct-zol RNA Miniprep Kit (Zymo Research, R2052, Irvine, CA, USA). cDNA was synthesized from 3 µg of RNA using TOPscript RT drymix (Enzynomics, RT200, Daejeon, Korea). qRT-PCR was performed using SYBR Green Master Mix (Enzynomics, RT500U), and gene expression was normalized to β-actin or RPLP0.

CRBN knockout and siRNA transfection

CRBN knockout was performed in HEK293T, U87, H1299, and Caki-1 cells using a CRISPR/Cas9 system (Santa Cruz, sc-412142). sgCRBN/Cas9 and HDR plasmids were transfected with FuGENE, and puromycin selection was applied after 24 h. For siRNA, cells were transfected with 10 nM CRBN siRNA (GenePharma, Suzhou, China) using FuGENE, and protein knockdown was confirmed by immunoblotting after 48 h.

Lentivirus production and transduction

shRNA plasmids against 6PGD in pGIPz and controls were purchased from Open Biosystems (Huntsville, AL, USA). Lentiviral particles were produced by co-transfecting shRNA, PAX2, and pMD2.G into HEK293FT cells. Viral supernatants were harvested at 48 h and concentrated using PEG-it. Target cells were transduced with polybrene (8 µg/mL) and selected with puromycin (1 µg/mL) for 2 weeks. Knockdown was verified by Western blot.

NADPH and 6PGD activity assays

NADPH/$NADP^+$ ratios were determined using a glucodehydrogenase cycling assay at 565 nm [19]. For 6PGD activity, 15 µg of lysate was added to assay buffer (50 mM Tris-HCl, pH 8.0; 0.1 mM $NADP^+$; 1 mM $MgCl_2$; 0.2 mM 6-phosphogluconate). NADPH production was measured at 340 nm every 20 s for 10 min using a DU800 Spectrophotometer (Beckman Coulter, Brea, CA, USA).

RNA sequencing and analysis

Total RNA (100 ng) was prepared using the Direct-zol kit. Sequencing reads were trimmed using Trim Galore (v1.18) and aligned to GRCh38 using STAR (v2.7.1a). FeatureCounts (v2.0.0) and Ensembl v101 annotations were used for quantification. Gene counts were normalized using RLE normalization.

Migration and invasion assays

For migration, PC3 and DU145 cells were seeded (1×10^6 cells/well, 6-well plates), and confluent monolayers were scratched with a 200 µL pipette tip. After washing, cells were cultured in fresh medium, and wound closure was monitored using ImageJ. For invasion, Transwell chambers (SPL, 35224, Pocheon, Korea) were coated with Matrigel (BD Biosciences, 354230, San Diego, CA, USA), and 1×10^6 cells were seeded in serum-free

medium. After 18–36 h, invaded cells were fixed, stained with crystal violet, and quantified under a microscope (five fields/sample).

Animal studies

WT and CRBN-KO mice (C57BL/6 background) were maintained under SPF conditions. Tissues were harvested, lysed, and analyzed by immunoblotting. All procedures were approved by the Asan Animal Care and Use Committee and Inha University Institutional Animal Care and Use Committee. The number of animals per group was determined based on prior studies using similar in vivo metastasis models, ensuring sufficient biological replicates for robust and consistent phenotype assessment. Animals were randomly assigned to control and experimental groups to minimize selection bias. Blinding was not feasible due to the nature of the experimental procedures; however, outcome measurements were conducted according to predefined quantitative criteria to mitigate potential bias.

Splenic metastasis model

All procedures were approved by the Asan Institute IACUC (2020-13-195). NRG mice (6-week-old males) were anesthetized, and DU145 or PC3 cells were injected into the spleen (5×10^5 or 1×10^6 cells/mouse, respectively). Tumors were monitored until the humane endpoint. Livers were weighed, frozen, or fixed in 10% NBF for histology.

Tail vein-lung metastasis model

All procedures were approved by the Inha University IACUC. BALB/c nu/nu mice of 6–8 weeks old were purchased from Orient Bio-Inc. A total of 2.5×10^6 human cells (Du145, Du145 CRBN, PC3, and PC3 CRBN) in 100 µL of phosphate-buffered saline (PBS) were slowly injected into mice through the tail vein to establish the mouse lung metastasis model of prostate cancer 16 weeks after injection; the lungs were fixed in Bouin's solution for the quantification of visible metastatic tumor nodules. Lungs were processed for hematoxylin and eosin (H&E) staining.

Protein structure refinement

Crystal structures of 6PGD (PDB: 4GWK) and CRBN (PDB: 4TZ4) were obtained from RCSB. Ligands and DDB1 were removed. Missing residues were modeled with Modeller 9.20 via ModWeb and ModLoop [23]. Structures were minimized using GROMACS 5.1.6 with added H-atoms and evaluated using QMean4 [24, 25].

Molecular docking

ClusPro 2.0, GRAMM-X, and FireDock [23, 26, 27] were used for rigid-body docking of CRBN and 6PGD. Binding models with favorable energetics and no steric clashes were selected for further simulation.

Molecular dynamics simulations

GROMACS 5.1.6 with Amber-03 force field was used [24]. Solvated boxes (TIP3P water, 0.1 M NaCl) were equilibrated via NVT and NPT (500 ps each), followed by 10 ns production runs. The last 5 ns were analyzed.

Binding energy calculation

FoldX was used to calculate binding free energies from 5-ns MD trajectories. Energetic terms included Van der Waals, solvation, electrostatics, entropy, and steric interactions [28].

Hotspot and interface analysis

Clustered MD frames (cutoff 0.25 nm) were analyzed by Robetta (CASM) for hotspot identification [29]. ConSurf and SPPIDER were used to identify evolutionarily conserved and interface residues [30].

Bioinformatic analysis

Publicly available transcriptomic datasets from prostate cancer patient specimens and normal prostate tissues were analyzed to evaluate CRBN and 6PGD mRNA expression patterns. RNA-seq data were obtained from the GDC TCGA-PRAD cohort (tumor, $n = 502$; normal, $n = 52$), the TCGA-PRAD PanCancer Atlas cohort ($n = 493$), and the SU2C/PCF metastatic prostate cancer cohort ($n = 208$). In addition, microarray data from the GEO database (GSE32571; tumor, $n = 59$; normal, $n = 39$) were included for independent validation. The GDC TCGA-PRAD and GSE32571 datasets were used to compare CRBN and 6PGD mRNA expression levels between prostate cancer and normal prostate tissues, whereas the TCGA-PRAD Pancancer Atlas and SU2C/PCF datasets were used to examine correlations between CRBN and 6PGD transcript levels in prostate cancer specimens.

Quantification and statistical analysis

Data are presented as mean ± SD from three independent experiments. Two-tailed unpaired Student's *t* tests, Spearman correlation analysis, or two-way ANOVA tests were performed using Microsoft Excel and PRISM. $^*p < 0.05$, $^{**}p < 0.01$, $^{***}p < 0.001$, and $^{****}p < 0.0001$ were considered statistically significant.

RESULTS

CRBN regulates 6PGD protein stability via ubiquitin-proteasome-dependent degradation

To evaluate the potential regulatory interaction between CRBN and 6PGD, we first generated CRBN-knockout (KO) HEK293T cell lines using the CRISPR/Cas9 system. HEK293T cells were selected for their high transfection efficiency, enabling robust exogenous protein expression suitable for mechanistic characterization. In this model, CRBN loss resulted in an approximately 1.7-fold increase in 6PGD protein, without affecting 6PGD mRNA levels (Fig. 1A, B). Reintroduction of wild-type CRBN into these KO cells successfully restored 6PGD protein levels, confirming a post-translational regulation mediated by CRBN (Fig. 1A).

To elucidate the underlying mechanism, wild-type cells were treated with MLN4924, a neddylation inhibitor of CRL4 activity, or MG132, a proteasome inhibitor. Both treatments triggered an accumulation of 6PGD protein, implicating CRL4 complex-mediated proteasomal degradation in 6PGD turnover (Fig. 1C). Cycloheximide chase assays further demonstrated that 6PGD stability was significantly prolonged in CRBN-deficient cells compared to wild-type controls (Fig. 1D).

To determine whether CRBN physically interacts with 6PGD, we performed co-immunoprecipitation (co-IP) assays. Both endogenous and overexpression-based co-IPs confirmed a direct interaction between CRBN and 6PGD (Fig. 1E and Fig. S1A). Immunoprecipitation with DDB1 further demonstrated that 6PGD is recruited to the $CRL4^{CRBN}$ complex (Fig. 1E and Fig. S1A). Notably, DDB1 co-immunoprecipitated Flag-tagged 6PGD in wild-type but failed to do so in CRBN-KO cells (Fig. S1B), indicating that CRBN is the essential substrate receptor recruiting 6PGD to the CRL4 E3 ligase complex.

To assess whether this interaction leads to polyubiquitination, we performed in vivo ubiquitination assays. Robust HA-tagged ubiquitin incorporation onto 6PGD was observed in wild-type cells, whereas CRBN-deficient cells showed diminished polyubiquitination (Fig. 1F). Re-expression of CRBN in KO cells restored 6PGD ubiquitination (Fig. 1G), and pretreatment with MLN4924 significantly attenuated 6PGD polyubiquitination (Fig. 1H), validating the requirement for CRL4 activity. Finally, we examined the impact of immunomodulatory drugs (IMiDs) on the CRBN-6PGD interaction. Interestingly, CRBN maintained its interaction with 6PGD in the presence of IMiDs, consistent with prior observations for glutamine synthetase (GS) (Fig. S1C) [22]. This interaction was also preserved with the IMiD-binding–deficient mutant $CRBN^{Y384A/W386A}$ (Fig. S1D) [11], and IMiD treatment did not affect CRBN-dependent 6PGD polyubiquitination (Fig. S1E). Collectively, these data establish that CRBN functions as a physiological E3 ligase receptor for 6PGD, promoting its ubiquitination and degradation independently of the IMiD.

CRBN recognizes the C-terminal domain of 6PGD to mediate ubiquitination and degradation

To map the structural determinants of CRBN recognition, we generated truncated 6PGD constructs corresponding to its

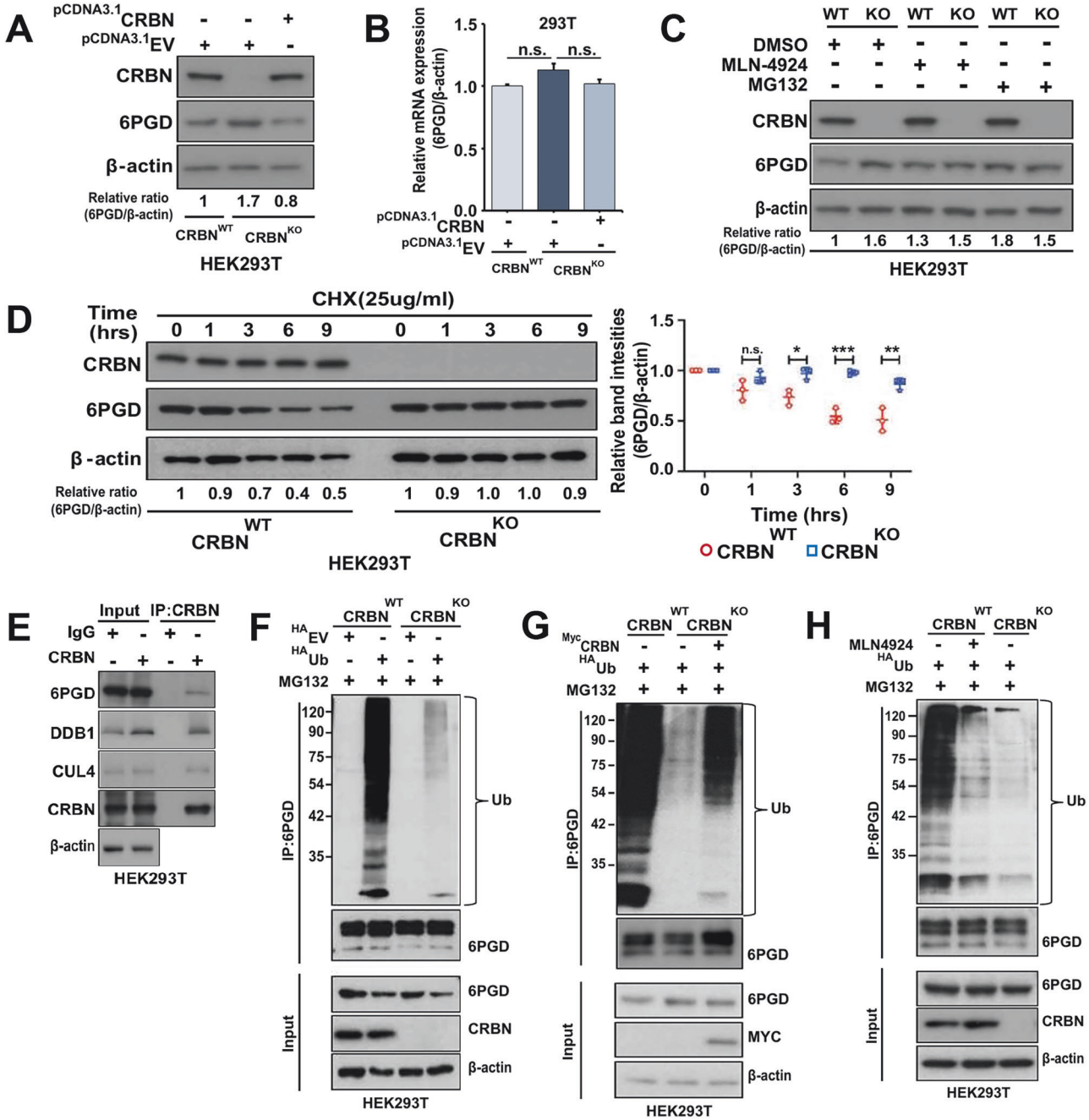

Fig. 1 CRBN regulates 6PGD protein expression through ubiquitination and proteasomal degradation. A Immunoblot analysis of CRBN and 6PGD expression in wild-type (WT) and CRBN-knockout (KO) HEK293T cells. CRBN was reintroduced into CRBN-KO cells. Relative 6PGD:β-actin ratios, normalized to WT control, are indicated. **B** qRT-PCR analysis of 6PGD mRNA levels in CRBN-KO HEK293T cells following CRBN knockout or ectopic CRBN expression. Values were normalized to β-actin. Data represent the mean ± SD of three independent replicates; n.s., not significant. **C** Immunoblot showing increased 6PGD protein levels upon proteasome or NEDD8-activating enzyme inhibition. WT and CRBN-KO cells were treated with MG132 (200 nM, 12 h) or MLN4924 (10 μM, 3 h). Relative 6PGD:β-actin ratios are shown. **D** Cycloheximide (CHX) chase assay assessing 6PGD protein stability. Immunoblot and quantification of 6PGD expression at the indicated time points; values were normalized to the 0 h time point. **E** Endogenous co-immunoprecipitation showing interaction of 6PGD with CRBN, CUL4, and DDB1. Lysates were immunoprecipitated with IgG or anti-CRBN and analyzed by immunoblotting. **F** CRBN-dependent polyubiquitination of 6PGD *via* the $CRL4^{CRBN}$ complex. WT and CRBN-KO cells were transfected with the indicated plasmids, treated with MG132 (10 μM, 3 h), and subjected to denaturing immunoprecipitation of 6PGD. Ubiquitination was detected with anti-HA. **G** Ectopic CRBN expression restores 6PGD ubiquitination in CRBN-KO cells. HA-ubiquitin and 6PGD were analyzed as in (**F**). **H** MLN4924 treatment abrogates 6PGD ubiquitination. Cells were co-treated with MLN4924 and MG132, and analyzed as in (**F**).

N-terminal (6PGD-NT) and C-terminal (6PGD-CT) domains (Fig. 2A). Co-immunoprecipitation (co-IP) assays revealed that CRBN selectively interacts with the C-terminal domain of 6PGD (Fig. 2B). Sequence alignment of this region identified a highly conserved α-helical motif containing residues Tyr449 and Phe450, which are conserved from yeast to humans (Fig. S2A).

To further define the molecular basis of the CRBN–6PGD interaction, we applied a computational modeling pipeline

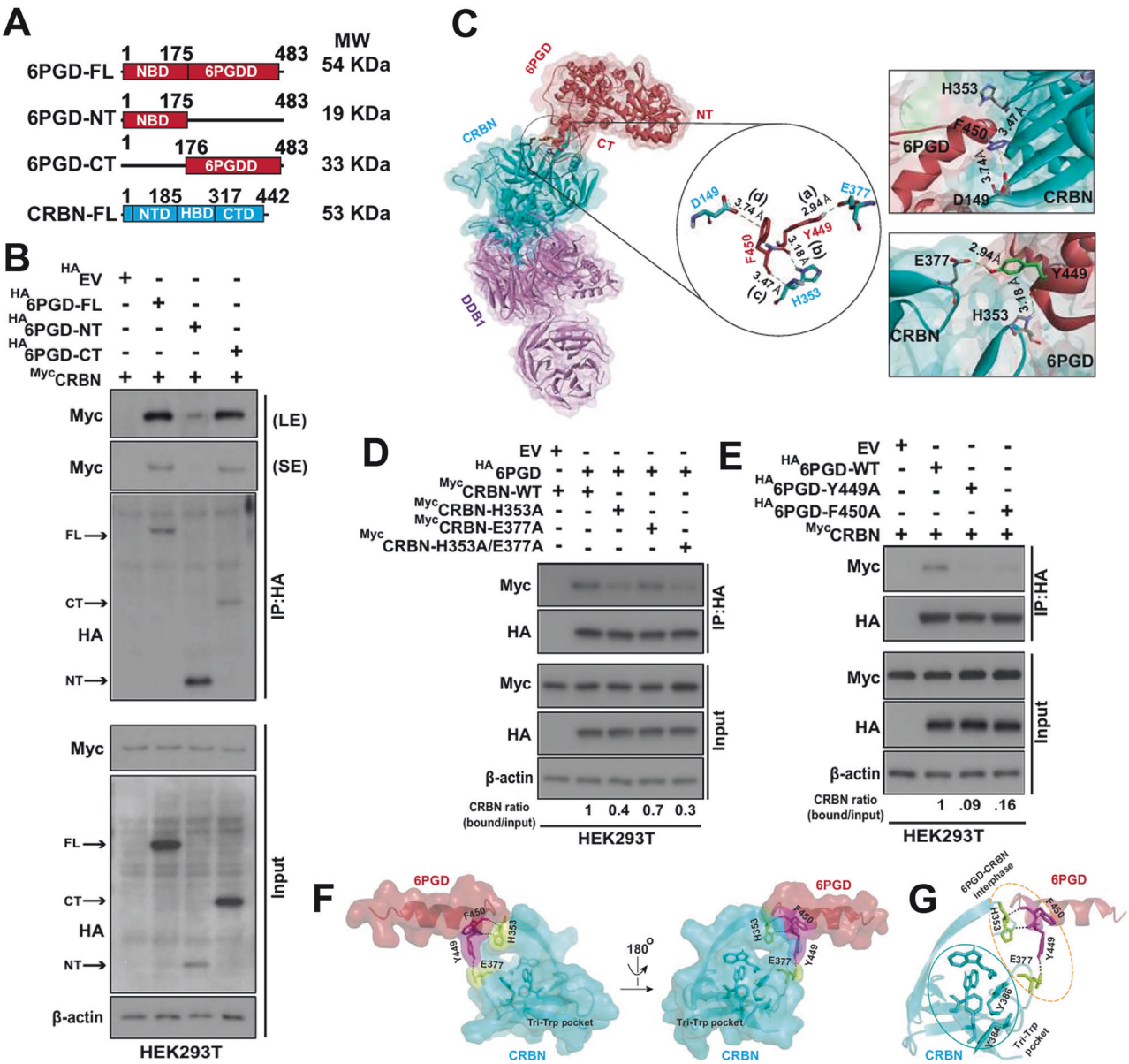

Fig. 2 CRBN recognizes the C-terminal domain of 6PGD to mediate ubiquitination and degradation. A Schematic representation of CRBN and 6PGD constructs used in this study. CRBN full-length (CRBN-FL) contains the N-terminal domain (NTD), helical bundle domain (HBD), and C-terminal domain (CTD). 6PGD full-length (6PGD-FL) includes the nucleotide-binding domain (NBD) and catalytic domain. **B** Co-immunoprecipitation (Co-IP) assay demonstrating that the C-terminal domain of 6PGD is necessary for binding to CRBN. **C** Predicted docking model of the 6PGD–CRBN complex based on molecular dynamics simulations, using 6PGD (PDB ID: 4GWK) and CRBN (PDB ID: 4TZ4). **D**, **E** Alanine substitution of key residues in CRBN (H353A, E377A) and 6PGD (Y449A, F450A) disrupts their interaction. **B**, **D**, **E** HEK293T cells were transfected with the indicated constructs, and lysates were subjected to HA immunoprecipitation followed by immunoblotting. Representative results from two or three independent experiments are shown. **F** Molecular interaction model showing CRBN residues H353 and E377 engaging with the α-helical motif (residues 438–453) in the 6PGD C-terminal region. **G** The predicted 6PGD–CRBN binding interface (dotted circle) is spatially distinct from the known CRBN–IMiD binding pocket (solid circle).

integrating the Binding Estimation After Refinement (BEAR) protocol, molecular docking, molecular dynamics (MD) simulations, and free energy calculations [23, 24, 26–28]. These analyses predicted multiple high-affinity binding modes between CRBN and 6PGD (Fig. S2B), identified the putative docking interface (Fig. 2C and Fig. S2C), and highlighted key interacting residues (Supplementary Tables 1 and 2).

These predictions were experimentally validated through alanine-substitution mutagenesis. Co-IP assays demonstrated that the CRBN^{H353A}, CRBN^{E377A}, and CRBN$^{H353A/E377A}$ double mutant reduced 6PGD binding to 0.4-, 0.7-, and 0.3-fold of control, respectively (Fig. 2D). Correspondingly, mutations at Tyr449 or Phe450 of 6PGD (6PGD^{Y449A} and 6PGD^{F450A}) completely abolished interaction with CRBN (Fig. 2E). Structural modeling confirmed that the CRBN–6PGD interface is spatially distinct from the IMiD-binding pocket (Fig. 2F), consistent with our earlier findings that neither IMiDs nor the CRBN$^{Y384A/W386A}$ mutant affected this interaction (Fig. S1C–E).

To assess the functional relevance of these interface residues, we performed ubiquitination assays. Only wild-type CRBN restored 6PGD polyubiquitination in CRBN-deficient cells (Fig. S2D), whereas interface-disrupting mutations in either CRBN or 6PGD

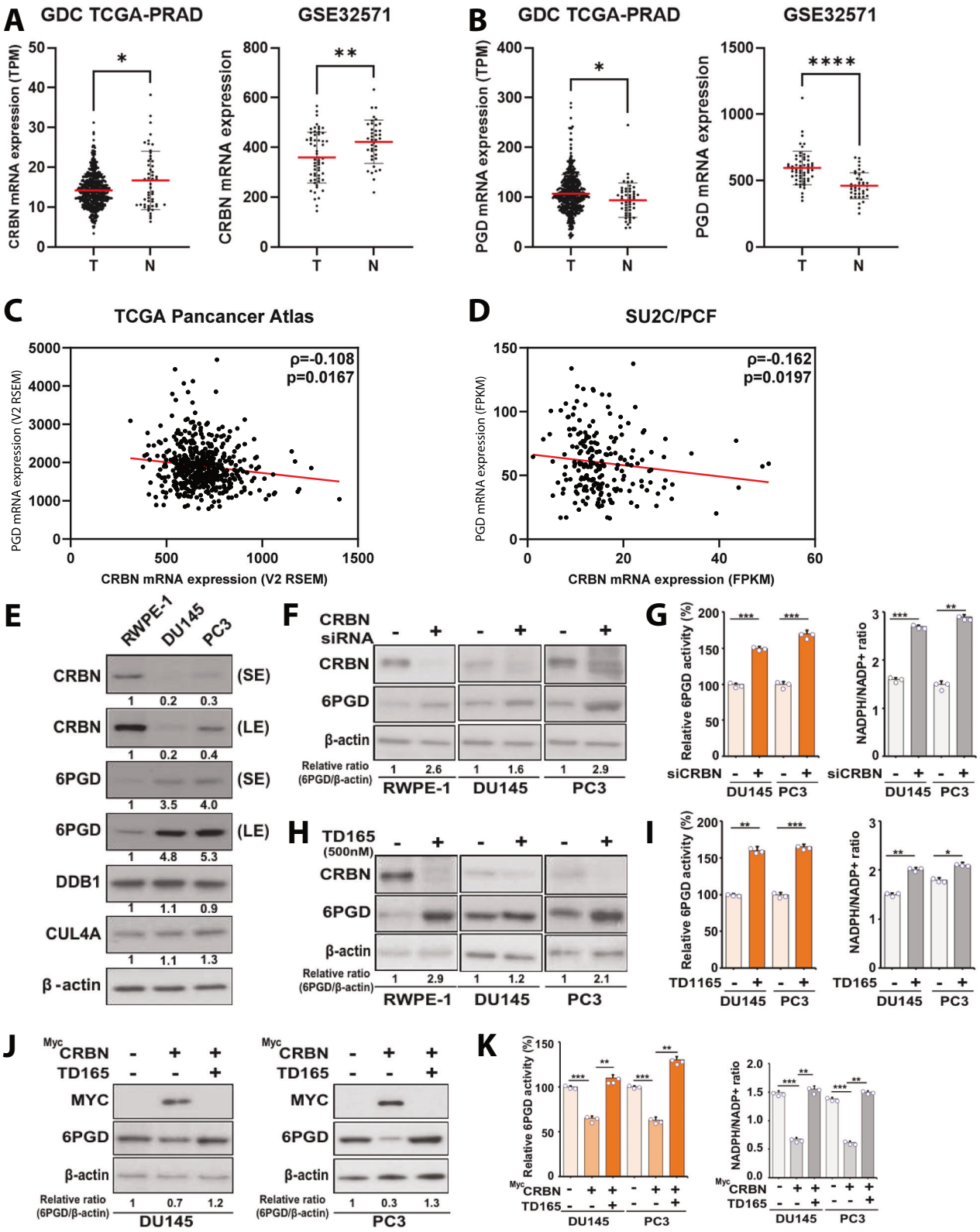
A
GDC TCGA-PRAD
GSE32571
CRBN mRNA expression (TPM)
CRBN mRNA expression
T
N
B
GDC TCGA-PRAD
GSE32571
PGD mRNA expression (TPM)
PGD mRNA expression
C
TCGA Pancancer Atlas
ρ=-0.108
p=0.0167
PGD mRNA expression (V2 RSEM)
CRBN mRNA expression (V2 RSEM)
D
SU2C/PCF
ρ=-0.162
p=0.0197
PGD mRNA expression (FPKM)
CRBN mRNA expression (FPKM)
E
RWPE-1
DU145
PC3
CRBN (SE)
CRBN (LE)
6PGD (SE)
6PGD (LE)
DDB1
CUL4A
β-actin
F
CRBN siRNA
CRBN
6PGD
β-actin
Relative ratio (6PGD/β-actin)
RWPE-1
DU145
PC3
G
Relative 6PGD activity (%)
NADPH/NADP+ ratio
siCRBN
DU145
PC3
H
TD165 (500nM)
CRBN
6PGD
β-actin
Relative ratio (6PGD/β-actin)
RWPE-1
DU145
PC3
I
Relative 6PGD activity (%)
NADPH/NADP+ ratio
TD1165
TD165
DU145
PC3
J
Myc
CRBN
TD165
MYC
6PGD
β-actin
Relative ratio (6PGD/β-actin)
DU145
PC3
K
Relative 6PGD activity (%)
NADPH/NADP+ ratio
Myc CRBN
TD165
DU145
PC3

Fig. 3 CRBN modulates 6PGD protein abundance and enzymatic activity in prostate cancer cells. Analysis of GDC TCGA-PRAD cohort and GSE32571 prostate cancer cohort showing reduced CRBN mRNA expression **A** and elevated 6PGD mRNA expression **B** in prostate cancer patient tissues compared with normal prostate tissues. *$p < 0.05$; **$p < 0.01$; ****$p < 0.0001$. **C, D** Scatter plots demonstrating a weak negative correlation between CRBN and 6PGD mRNA expression in prostate cancer patient samples from the TCGA-PRAD (Pancancer Atlas) cohort **C** and the SU2C/PCF metastatic prostate cancer cohort (**D**). **E** Western blot analysis showing reduced CRBN and elevated 6PGD protein expression in DU145 and PC3 prostate cancer cells compared to the normal prostate epithelial cell line RWPE-1. CRBN silencing via siRNA increases 6PGD protein levels **F**, enzymatic activity, and intracellular NADPH/$NADP^+$ ratio **G** in RWPE-1, DU145, and PC3 cells. Pharmacological degradation of CRBN using TD165 (500 nM, 12 h) elevates 6PGD protein abundance **H**, activity, and NADPH/$NADP^+$ levels (**I**). Ectopic expression of CRBN decreases 6PGD protein levels **J**, enzymatic activity, and NADPH/$NADP^+$ ratio **K**; these effects are further enhanced by TD165 treatment. Data represent the mean ± SD of biological replicates. *$p < 0.05$; **$p < 0.01$; ***$p < 0.001$.

significantly impaired ubiquitin conjugation (Fig. S2E). Collectively, these results demonstrate that CRBN specifically recognizes the C-terminal α-helical motif of 6PGD *via* residues H353 and Glu377, interacting with 6PGD residues Tyr449 and Phe450 to trigger polyubiquitination and proteasomal degradation.

CRBN modulates 6PGD protein abundance and enzymatic activity in prostate cancer cells

To investigate the clinical relevance of the CRBN-6PGD axis, we analyzed publicly available patient datasets, including GDC TCGA-PRAD and an independent GEO dataset (GSE32571). Across these cohorts, we consistently observed a significant reduction in CRBN mRNA expression and an increase in 6PGD mRNA expression in prostate cancer tissues compared with normal prostate tissues (Fig. 3A, B). Further analysis of the TCGA-PRAD (Pancancer Atlas) cohort and the SU2C/PCF metastatic prostate cancer cohort revealed a weak negative correlation between CRBN and 6PGD transcripts in patient samples (Fig. 3C, D). Guided by these clinical observations, we next examined the regulatory relationship between CRBN and 6PGD in prostate cancer cell lines. 6PGD protein levels were elevated to 3.5- and 4.0-fold of control in DU145 and PC3 cells, and the intracellular NADPH/$NADP^+$ ratios were significantly elevated relative to the non-malignant prostate epithelial cell line RWPE-1. Importantly, these protein-level changes occurred without corresponding alterations in 6PGD mRNA expression, supporting a consistent post-translational mode of regulation that parallels our observations in the HEK293T cells (Fig. 3E and Fig. S3A, B). In contrast, the expression levels of other $CRL4^{CRBN}$ complex components, including DDB1 and CUL4A, remained consistent between normal and cancerous cell lines (Fig. 3E).

To validate the functional consequence of CRBN loss, we depleted CRBN using either siRNA or TD165, a CRBN-specific proteolysis-targeting chimera (PROTAC) [31]. Both approaches significantly increased 6PGD protein levels, enzymatic activity, and intracellular NADPH/$NADP^+$ ratios across DU145 and PC3 cells (Fig. 3F–I), again without altering 6PGD mRNA expression (Fig. S3C, D). Conversely, transient overexpression of Myc-tagged CRBN reduced both 6PGD protein levels and enzymatic activity, effects that were rescued by TD165 treatment (Fig. 3J, K). Together, these findings confirm that CRBN governs 6PGD abundance and metabolic activity in prostate cancer cells via post-translational control.

CRBN suppresses AR-negative prostate cancer cell metastasis in vitro and in vivo

To investigate the functional role of CRBN in prostate cancer progression, we established DU145 and PC3 cell lines with stable retroviral overexpression of CRBN (CRBN EE) (Fig. S4A). CRBN overexpression significantly attenuated the migratory and invasive capacities of both cell lines in vitro (Fig. 4A, B), without affecting cell proliferation (Fig. S4B), suggesting a specific defect in metastatic potential rather than general growth.

To assess the metastatic burden in vivo, we utilized two xenograft models. In an intra-splenic model using immunodeficient NRG mice, the CRBN EE group exhibited significantly lower liver-to-body ratios and fewer metastatic liver lesions compared to controls (Fig. 4C and Fig. S4C). Similarly, in a tail vein injection model, CRBN EE cells exhibited significantly reduced formation of metastatic lung nodules, confirmed by H&E staining (Fig. S4D, F). These data strongly support an anti-metastatic function of CRBN in prostate cancer.

To determine whether CRBN-mediated regulation of 6PGD is dependent on androgen receptor (AR) status, we pharmacologically reduced CRBN expression using TD165 treatment in the AR-positive prostate cancer cell line LNCaP and assessed functional outcomes using a wound healing assay. Although TD165 treatment effectively degraded CRBN, it failed to increase 6PGD protein levels or enhance migration in LNCaP cells (Fig. S4G, H). This clear difference suggests that the CRBN-6PGD axis and its impact on metastasis are specific to the AR-negative context, potentially due to distinct metabolic or signaling dependencies in AR-positive prostate cancer.

The CRBN–6PGD axis regulates EMT-related gene expression

To elucidate the molecular mechanisms linking CRBN to metastasis, we performed transcriptomic analysis of DU145 CRBN EE cells. RNA sequencing identified significant alterations of EMT markers, including upregulation of epithelial marker CDH1 (E-cadherin) and downregulation of the mesenchymal marker MMP1 (Fig. 5A and Table S3). These changes were validated by quantitative RT-PCR and western blotting (Fig. 5B, C).

To determine whether this transcriptional shift relies on the physical interaction between CRBN–6PGD, we introduced CRBN interface mutants (H353A and E377A) into DU145 and PC3 cells. Unlike wild-type CRBN, these mutants failed to modulate CDH1 and MMP1 expression (Fig. 5D), indicating that direct binding and degradation of 6PGD are required for CRBN-mediated EMT suppression.

Finally, to confirm that 6PGD enzymatic activity drives this phenotype, we treated CRBN-depleted cells (*via* TD165) with the 6PGD inhibitors physcion (P) and 6-aminonicotinamide (6-AN). Pharmacological inhibition of 6PGD activity reversed the TD165-induced suppression of CDH1 and induction of MMP1 (Fig. 5E). These results place 6PGD metabolic activity downstream of CRBN, acting as a driver of the EMT transcriptional program.

CRBN suppresses metastasis by limiting 6PGD stability and metabolic function

To comprehensively validate the functional sequence of this pathway, we correlated metabolic changes with invasive phenotypes. Expression of CRBN WT, but not the interface mutants, significantly reduced 6PGD enzymatic activity, lowered intracellular NADPH/$NADP^+$ ratios, and enhanced 6PGD polyubiquitination (Fig. 6A, B, and Fig. S5A). Consistently, CRBN WT-expressing cells displayed reduced migratory and invasive behavior in vitro, whereas CRBN mutants showed no reduction in metastatic behavior (Fig. 6C, D, and Fig. S5B). Furthermore, the enhanced migration and invasion caused by CRBN depletion (TD165) were effectively blocked by pharmacological inhibition of 6PGD (Fig. 6E–G and Fig. S5C–E). These findings confirm that CRBN suppresses prostate cancer cell migration and invasion specifically by destabilizing 6PGD and limiting its metabolic output.

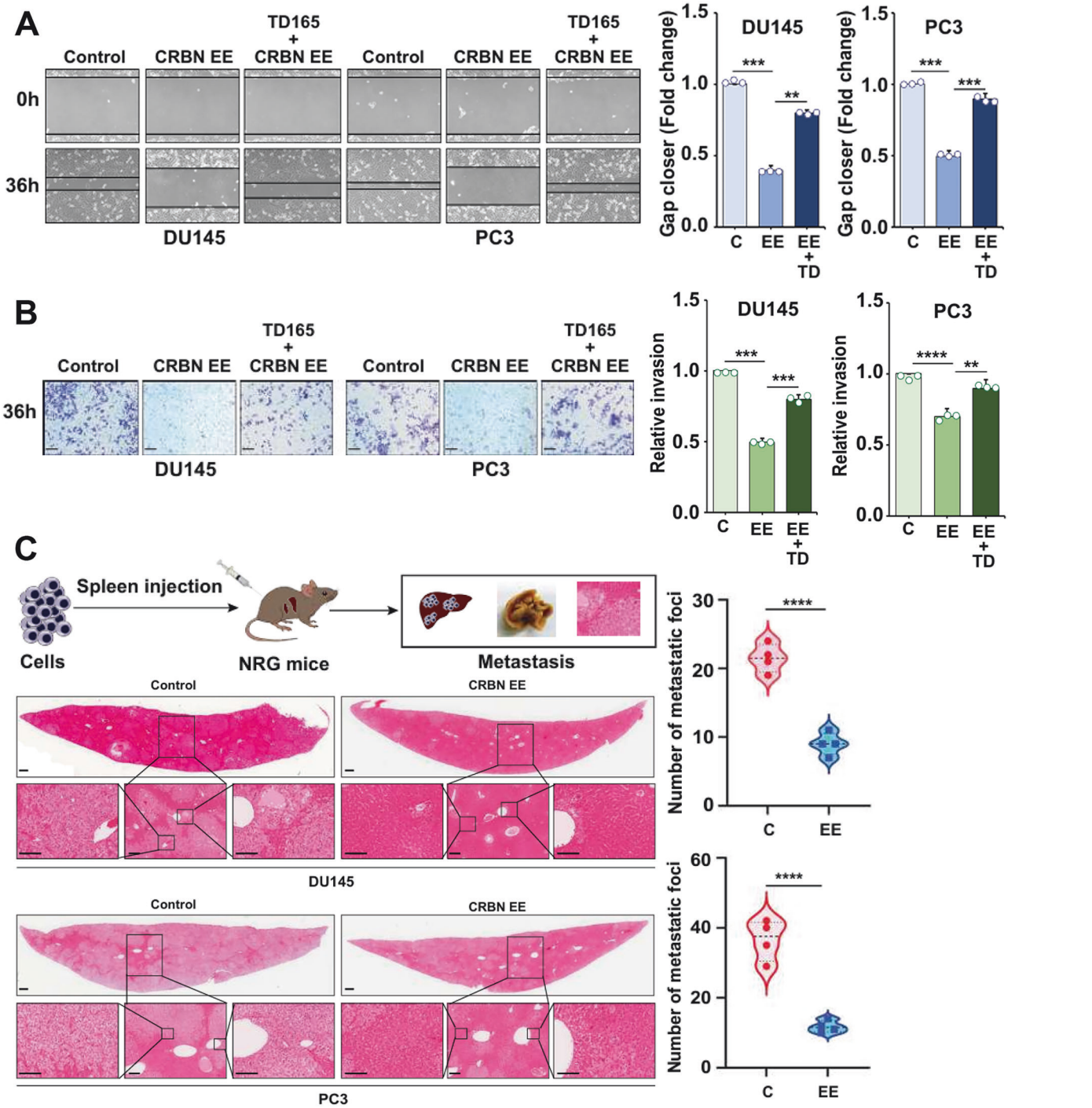

Fig. 4 Enforced CRBN expression suppresses prostate cancer metastasis in vitro and in vivo. Overexpression of CRBN significantly reduces cell migration **A** and invasion **B** in DU145 and PC3 cells; these effects are reversed by TD165 treatment. **C** Intra-splenic injection of CRBN-overexpressing (CRBN EE) DU145 and PC3 cells into NRG mice results in reduced liver metastases, as quantified by hematoxylin and eosin (H&E)-stained metastatic nodules. $n = 6$ mice per group. Data represent mean ± SD. $^{**}p < 0.01$; $^{***}p < 0.001$; $^{****}p < 0.0001$.

The CRBN–6PGD axis regulates cancer cell migration and invasion across multiple tumor types

Consistent with our prostate cancer models, CRBN-deficient mice exhibited elevated 6PGD protein levels in multiple tissues, including the brain, lung, and kidney (Fig. 7A and Fig. S6A). To test the universality of this mechanism, we deleted CRBN in HEK293T and mouse embryonic fibroblast (MEF). In both cell types, CRBN loss increased 6PGD protein abundance without altering mRNA (Fig. 7B and Fig. S6B).

Similar effects were observed in the human cancer cell lines U87 (glioblastoma), H1299 (non-small cell lung carcinoma), and Caki-1 (clear cell renal carcinoma) (Fig. 7C, D; Fig. S6C, D). In all cell lines tested, loss of CRBN significantly enhanced migration and invasion, and genetic knockdown or pharmacological inhibition of 6PGD suppressed these migratory and invasive phenotypes (Fig. 7E–H; Fig. S6E–G). These results demonstrate that the CRBN–6PGD axis functions as a broadly conserved regulatory node governing cancer cell motility and invasiveness across multiple tumor types.

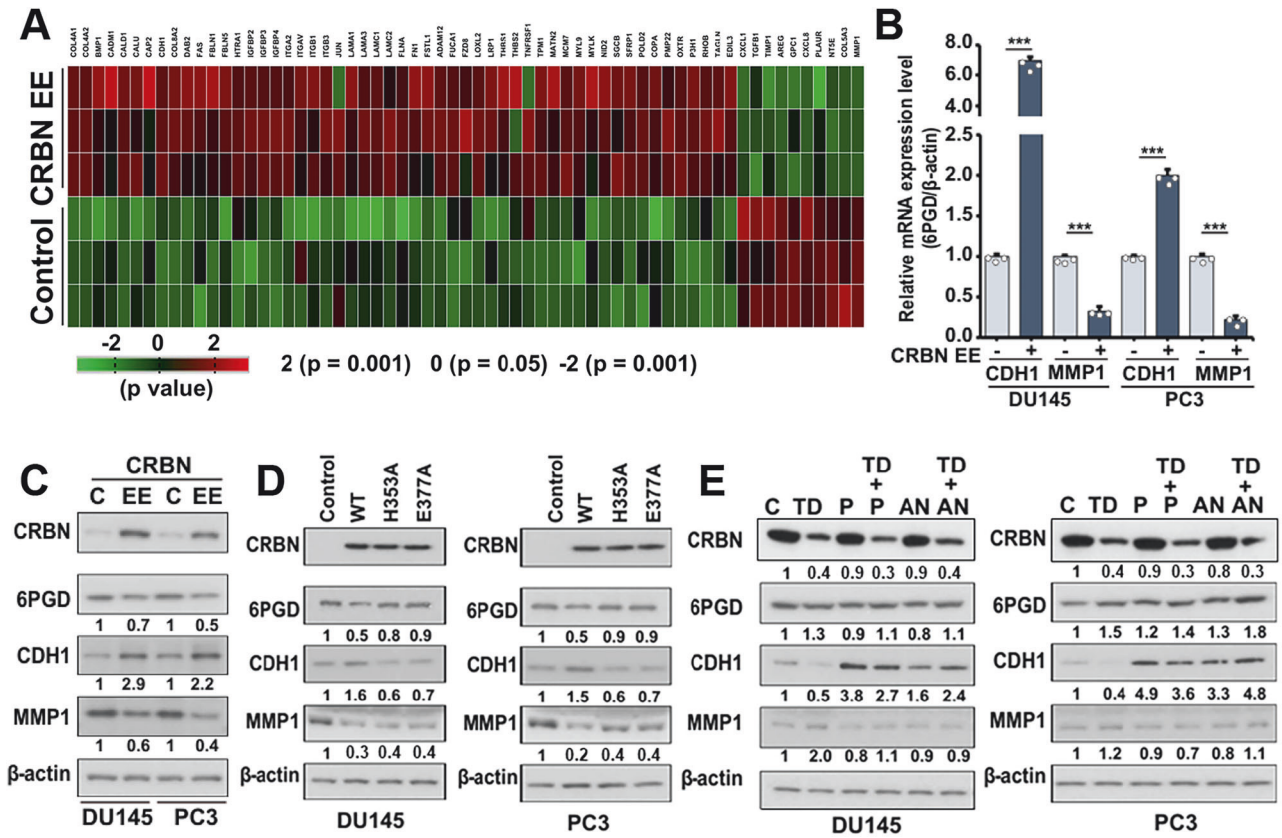

Fig. 5 The CRBN-6PGD axis regulates EMT-related gene expression. A Heatmap of RNA sequencing data showing differential expression of EMT-related genes in CRBN-overexpressing (CRBN EE) DU145 cells. **B** Quantitative RT-PCR analysis demonstrating that CRBN overexpression increases CDH1 and decreases MMP1 mRNA levels. ***$p < 0.001$. **C** Western blot analysis of EMT markers in CRBN EE versus control DU145 and PC3 cells. **D** Wild-type CRBN (CRBN-WT), but not 6PGD-binding-deficient mutants (H353A, E377A), modulates EMT marker protein levels. **E** TD165-induced changes in EMT marker expression are reversed by treatment with the 6PGD inhibitors physcion or 6-aminonicotinamide (6-AN). **C**–**E** β-actin was used as a loading control in panels.

DISCUSSION

Prostate cancer is one of the most common malignancies in men and remains a leading cause of cancer-related mortality worldwide [3, 32, 33]. Metastatic progression is the primary cause of death in patients with advanced disease [34]. Although androgen receptor (AR) signaling has long been the cornerstone of therapeutic intervention [35, 36], the emergence of resistance to AR-targeted agents underscores the urgent need for alternative strategies. In this context, metabolic reprogramming has gained increasing attention as a hallmark of cancer progression. Here, we identify a previously unrecognized regulatory axis in which cereblon (CRBN), a substrate adaptor of the $CRL4^{CRBN}$ E3 ubiquitin ligase complex, suppresses prostate cancer metastasis by promoting the degradation of 6-phosphogluconate dehydrogenase (6PGD), a key enzyme in the oxidative branch of the pentose phosphate pathway (oxPPP).

Functionally, 6PGD is a rate-limiting enzyme in the oxPPP, generating NADPH required for biosynthesis and redox homeostasis [37, 38]. NADPH plays a central role in supporting anabolic biosynthesis and maintaining redox balance—metabolic processes co-opted by cancer cells to fuel proliferation, buffer oxidative stress, and facilitate epithelial–mesenchymal transition (EMT), a key driver of metastatic plasticity [38–42]. Elevated 6PGD activity has been associated with increased tumor aggressiveness and poor clinical outcomes in multiple cancers, including prostate cancer [18, 43]. However, the upstream regulatory mechanisms controlling 6PGD protein stability have remained elusive.

Our findings resolve this by defining CRBN as the physiological E3 ligase substrate receptor for 6PGD. We demonstrate that CRBN directly binds a conserved C-terminal α-helical motif in 6PGD, promoting its polyubiquitination and proteasomal degradation independently of immunomodulatory drugs (IMiDs), thereby revealing a native substrate function distinct from CRBN's well-characterized pharmacological neo-substrate regulation.

The physiological consequences of this regulation are profound. CRBN loss leads to changes in 6PGD protein abundance, enzymatic activity, and intracellular NADPH/NADP ratio in prostate cancer. Beyond its metabolic effects, the CRBN-6PGD axis also regulates epithelial-mesenchymal plasticity, as CRBN overexpression upregulates CDH1 and downregulates MMP1, while pharmacologic inhibition of 6PGD is sufficient to override the transcriptional changes caused by TD165-mediated CRBN knockdown. These results demonstrate that CRBN-mediated 6PGD degradation influences both metabolic control and EMT-associated gene expression to drive metastatic behavior.

Importantly, our findings demonstrate that CRBN-mediated control of 6PGD is conserved in multiple cancer types, indicating that CRBN-directed therapies may have wider translational applicability beyond prostate cancer. More broadly, our study expands the biological scope of CRBN beyond its established IMiD-dependent activity in hematologic malignancies [10, 44] and positions CRBN as a metabolic gatekeeper in pan-cancer relevance.

These findings also carry translational implications. Based on the reciprocal expression patterns of CRBN and 6PGD mRNA

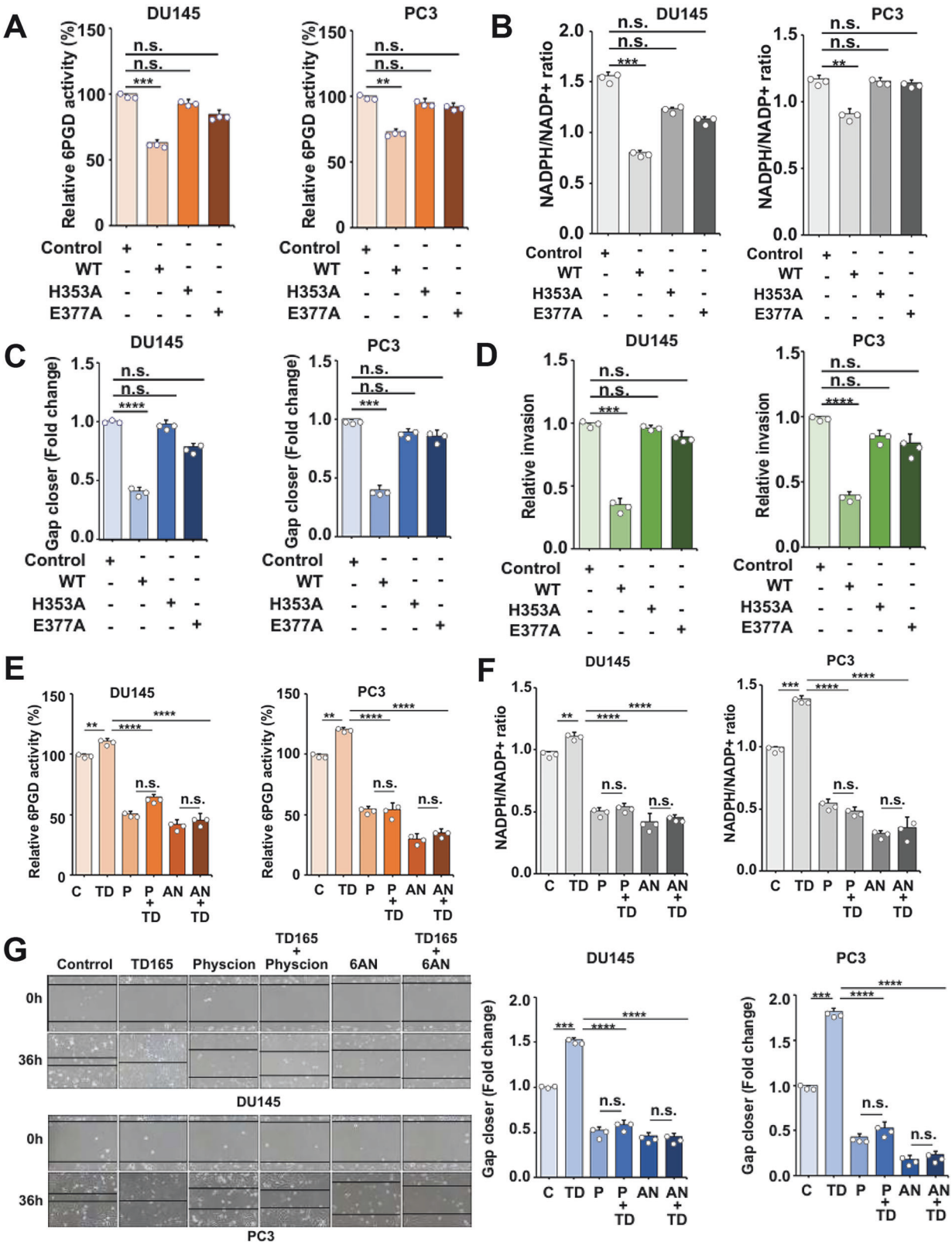

Fig. 6 CRBN regulates 6PGD stability and function to suppress prostate cancer metastasis. Expression of wild-type CRBN (CRBN-WT), but not binding-deficient mutants H353A and E377A, decreases 6PGD enzymatic activity **A** and the NADPH/NADP⁺ ratio **B** in DU145 and PC3 cells. $^{**}p < 0.01$; $^{***}p < 0.001$. CRBN-WT suppresses cell migration **C** and invasion **D**, whereas CRBN mutants fail to do so. $^{***}p < 0.001$; $^{****}p < 0.0001$. TD165-mediated CRBN degradation increases 6PGD activity **E** and NADPH/NADP⁺ ratios **F**; these effects are reversed by physcion or 6-aminonicotinamide (6-AN). $^{**}p < 0.01$; $^{****}p < 0.0001$. **G** Wound healing assays show enhanced migration upon CRBN loss, which is rescued by 6PGD inhibition. $^{***}p < 0.001$; $^{****}p < 0.0001$.

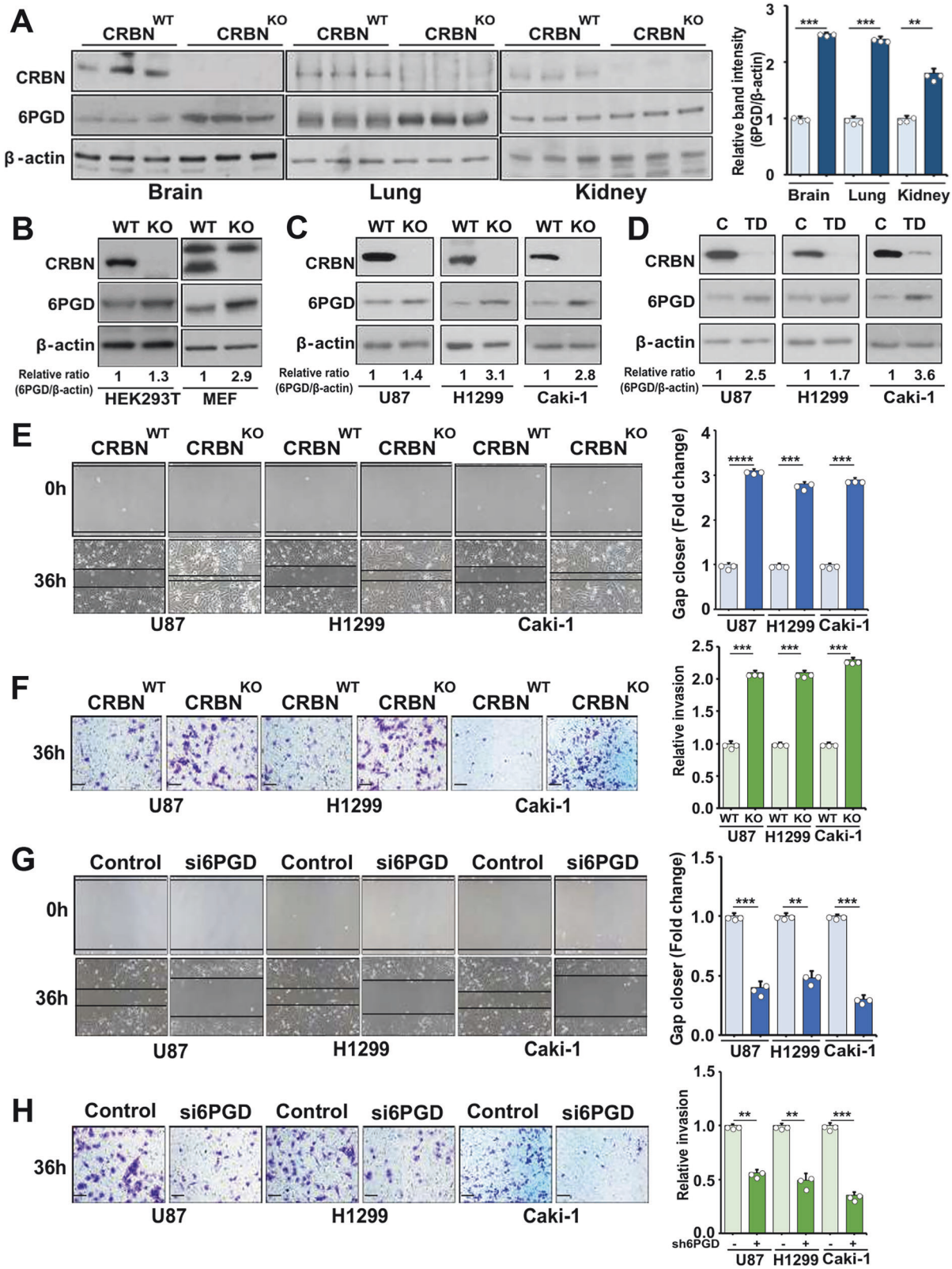

Fig. 7 The CRBN–6PGD axis regulates cancer cell migration and invasion across multiple tumor types. A Western blot analysis showing elevated 6PGD protein levels in brain, lung, and kidney tissues from CRBN knockout (KO) mice. $n = 3$ mice per group. $^{**}p < 0.01$; $^{***}p < 0.001$. **B**–**D** CRBN deletion or TD165 treatment increases 6PGD protein expression in HEK293T, mouse embryonic fibroblasts (MEFs), and multiple cancer cell lines, including U87 (glioblastoma), H1299 (lung carcinoma), and Caki-1 (renal carcinoma). CRBN KO enhances cell migration **E** and invasion **F** in U87, H1299, and Caki-1 cells. $^{***}p < 0.001$; $^{****}p < 0.0001$. siRNA-mediated knockdown or pharmacological inhibition of 6PGD reduces migration **G** and invasion **H** in the same cell lines. $^{**}p < 0.01$; $^{***}p < 0.001$.

observed in publicly available datasets, CRBN expression may serve as a prognostic biomarker in prostate cancer, with low CRBN levels indicative of elevated 6PGD levels and heightened metastatic risk. Although we did not evaluate primary tumor volume in vivo, our proliferation assays did not show any significant differences upon CRBN modulation, supporting a metastasis-specific function consistent with our in vivo findings.

Crucially, our data indicate that CRBN-mediated regulation of 6PGD and metastatic progression is context-dependent, being particularly relevant in AR-negative prostate cancer, a clinically more aggressive subtype with urgent therapeutic needs. In AR-positive LNCaP cells, the attenuated regulatory effects imply that AR signaling may dominate or compensate for CRBN-dependent 6PGD control and associated metabolic reprogramming [45, 46]. This observation raises the possibility that co-targeting the CRBN–6PGD axis together with AR signaling pathways may yield synergistic therapeutic benefits in AR-positive prostate cancer. In contrast, in AR-negative or AR-low/castration-resistant prostate cancer, where AR signaling is diminished, targeting the CRBN-6PGD axis alone may be more advantageous, particularly given the prominence of metabolic rewiring and lineage plasticity.

Therapeutically, this study suggests that stabilizing CRBN or activating its function could be more advantageous than direct 6PGD inhibition. While 6PGD inhibition alone suppresses oxidative PPP activity and tumor growth [43], it risks systemic toxicity due to the enzyme's essential role in normal physiology. Conversely, activating CRBN may offer a more selective strategy, as it regulates 6PGD through a context-dependent post-translational mechanism, leading to a preferential impact on tumor cells. Moreover, CRBN influences multiple downstream effectors and metabolic nodes [16, 22, 47–49], suggesting a broader capacity to modulate cancer-associated metabolic flux rather than solely suppressing a single enzymatic step.

However, we acknowledge certain limitations. Our clinical correlations rely on transcriptomic data, whereas our mechanistic findings define a protein-level regulation. Thus, transcript profiles may not fully capture the functional consequences of CRBN in prostate cancer, underscoring the need for future protein-level validation using patient tissues and immunohistochemical analyses. Additionally, it will be vital to explore whether this axis contributes to site-specific metastasis or immune evasion.

In summary, we establish the $CRL4^{CRBN}$ complex as a critical suppressor of the oxidative PPP and metastasis in prostate cancer. By targeting 6PGD for degradation, CRBN constrains the metabolic fuel required for EMT and invasion. Restoring CRBN function or targeting the downstream 6PGD axis offers a promising therapeutic strategy, particularly for aggressive, AR-negative prostate cancers driven by metabolic reprogramming. These regulatory mechanisms are conserved across multiple cancer types, highlighting the broad significance of CRBN in tumor biology.

DATA AVAILABILITY

The data of this study are available from the corresponding author upon reasonable request.

REFERENCES

1. Mucci LA, Wilson KM, Giovannucci EL. Epidemiology of prostate cancer. In: Pathology and Epidemiology of Cancer. Cham: Springer International Publishing; 2016. 107–25.
2. Ferlay J, Colombet M, Soerjomataram I, Parkin DM, Piñeros M, Znaor A, et al. Cancer statistics for the year 2020: an overview. Int J Cancer. 2021;149:778–89.
3. Elmehrath AO, Afifi AM, Al-Husseini MJ, Saad AM, Wilson N, Shohdy KS, et al. Causes of death among patients with metastatic prostate cancer in the US from 2000 to 2016. JAMA Netw Open. 2021;4:e2119568.
4. Fares J, Fares MY, Khachfe HH, Salhab HA, Fares Y. Molecular principles of metastasis: a hallmark of cancer revisited. Signal Transduct Target Ther. 2020;5:28.
5. Soe AM, Bordia S, Xiao PQ, Lopez-Morra H, Tejada J, Atluri S, et al. A rare presentation of metastasis of prostate adenocarcinoma to the stomach and rectum. J Gastric Cancer. 2014;14:271–4.
6. Kim HK, Seol JE, Ahn SW, Jeon S, Park CS, Han J. Cereblon: promise and challenges for combating human diseases. Pflügers Arch. 2021;473:1–17.
7. Kim HK, Ko TH, Nyamaa B, Lee SR, Kim N, Ko KS, et al. Cereblon in health and disease. Pflügers Arch. 2016;468:1299–309.
8. Fischer ES, Böhm K, Lydeard JR, Yang H, Stadler MB, Cavadini S, et al. Structure of the DDB1–CRBN E3 ubiquitin ligase in complex with thalidomide. Nature. 2014;512:49–53.
9. Zhou L, Xu G. Cereblon attenuates DNA damage-induced apoptosis by regulating the transcription-independent function of p53. Cell Death Dis. 2019;10:69.
10. Zhu YX, Braggio E, Shi CX, Kortuem KM, Bruins LA, Schmidt JE, et al. Identification of cereblon-binding proteins and relationship with response and survival after IMiDs in multiple myeloma. Blood. 2014;124:536–45.
11. Ito T, Ando H, Suzuki T, Ogura T, Hotta K, Imamura Y, et al. Identification of a primary target of thalidomide teratogenicity. Science. 2010;327:1345–50.
12. Lopez-Girona A, Mendy D, Ito T, Miller K, Gandhi AK, Kang J, et al. Cereblon is a direct protein target for immunomodulatory and antiproliferative activities of lenalidomide and pomalidomide. Leukemia. 2012;26:2326–35.
13. Beedie SL, Huang PA, Harris EM, Strope JD, Mahony C, Chau CH, et al. Role of cereblon in angiogenesis and in mediating the antiangiogenic activity of immunomodulatory drugs. FASEB J. 2020;34:11395–404.
14. Kim MJ, Min Y, Shim JH, Chun E, Lee KY. CRBN is a negative regulator of bactericidal activity and autophagy activation through inhibiting the ubiquitination of ECSIT and BECN1. Front Immunol. 2019;10:2203.
15. Kim MJ, Lee JS, Kim JY, Choi B, Son J, Min Y, et al. CRBN is downregulated in lung cancer and negatively regulates TLR2, 4 and 7 stimulation in lung cancer cells. Clin Transl Med. 2022;12:e1050.
16. Shin S, Cho SK. CRBN deletion enhances mitochondrial metabolism by stimulating mitochondrial calcium accumulation in non-small cell lung cancer. Life Sci. 2025;364:123444.
17. Sarfraz I, Rasul A, Hussain G, Shah MA, Zahoor AF, Asrar M, et al. 6-Phosphogluconate dehydrogenase fuels multiple aspects of cancer cells: From cancer initiation to metastasis and chemoresistance. Biofactors. 2020;46:550–62.
18. Lin R, Elf S, Shan C, Kang HB, Ji Q, Zhou L, et al. 6-Phosphogluconate dehydrogenase links oxidative PPP, lipogenesis and tumour growth by inhibiting LKB1–AMPK signalling. Nat Cell Biol. 2015;17:1484–96.
19. Shan C, Elf S, Ji Q, Kang HB, Zhou L, Hitosugi T, et al. Lysine acetylation activates 6-phosphogluconate dehydrogenase to promote tumor growth. Mol Cell. 2014;55:552–65.
20. Liu R, Li W, Tao B, Wang X, Yang Z, Zhang Y, et al. Tyrosine phosphorylation activates 6-phosphogluconate dehydrogenase and promotes tumor growth and radiation resistance. Nat Commun. 2019;10:991.
21. Chan B, VanderLaan PA, Sukhatme VP. 6-Phosphogluconate dehydrogenase regulates tumor cell migration in vitro by regulating receptor tyrosine kinase c-Met. Biochem Biophys Res Commun. 2013;439:247–51.
22. Nguyen TV, Lee JE, Sweredoski MJ, Yang SJ, Jeon SJ, Harrison JS, et al. Glutamine triggers acetylation-dependent degradation of glutamine synthetase *via* the thalidomide receptor cereblon. Mol Cell. 2016;61:809–20.
23. Kozakov D, Hall DR, Xia B, Porter KA, Padhorny D, Yueh C, et al. The ClusPro web server for protein–protein docking. Nat Protoc. 2017;12:255–78.
24. Hess B, Kutzner C, van der Spoel D, Lindahl E. GROMACS 4: algorithms for highly efficient, load-balanced, and scalable molecular simulation. J Chem Theory Comput. 2008;4:435–47.
25. Benkert P, Biasini M, Schwede T. Toward the estimation of the absolute quality of individual protein structure models. Bioinformatics. 2011;27:343–50.
26. Tovchigrechko A, Vakser IA. GRAMM-X public web server for protein–protein docking. Nucleic Acids Res. 2006;34:W310–4.
27. Mashiach E, Schneidman-Duhovny D, Andrusier N, Nussinov R, Wolfson HJ. FireDock: a web server for fast interaction refinement in molecular docking. Nucleic Acids Res. 2008;36:W229–32.
28. Schymkowitz J, Borg J, Stricher F, Nys R, Rousseau F, Serrano L. The FoldX web server: an online force field. Nucleic Acids Res. 2005;33:W382–8.
29. Kortemme T, Kim DE, Baker D. Computational alanine scanning of protein-protein interfaces. Sci STKE. 2004;2004:pl2.
30. Glaser F, Pupko T, Paz I, Bell RE, Bechor-Shental D, Martz E, et al. ConSurf: identification of functional regions in proteins by surface-mapping of phylogenetic information. Bioinformatics. 2003;19:163–4.
31. Kim K, Lee DH, Park S, Jo SH, Ku B, Park SG, et al. Disordered region of cereblon is required for efficient degradation by proteolysis-targeting chimera. Sci Rep. 2019;9:19654.

32. Wang L, Lu B, He M, Wang Y, Wang Z, Du L. Prostate cancer incidence and mortality: global status and temporal trends in 89 countries from 2000 to 2019. Front Public Health. 2022;10:811044.
33. Schafer EJ, Laversanne M, Sung H, Soerjomataram I, Briganti A, Dahut W, et al. Recent patterns and trends in global prostate cancer incidence and mortality: an update. Eur Urol. 2025;87:302–13.
34. Bray F, Laversanne M, Sung H, Ferlay J, Siegel RL, Soerjomataram I, et al. Global cancer statistics 2022: GLOBOCAN estimates of incidence and mortality worldwide for 36 cancers in 185 countries. CA Cancer J Clin. 2024;74:229–63.
35. Scher HI, Fizazi K, Saad F, Taplin ME, Sternberg CN, Miller K, et al. Increased survival with enzalutamide in prostate cancer after chemotherapy. N Engl J Med. 2012;367:1187–97.
36. de Bono JS, Logothetis CJ, Molina A, Fizazi K, North S, Chu L, et al. Abiraterone and increased survival in metastatic prostate cancer. N Engl J Med. 2011;364:1995–2005.
37. Rippa M, Signorini M, Dallocchio F. Differentiation between the structural and redox roles of TPNH in 6-phosphogluconate dehydrogenase. Biochem Biophys Res Commun. 1972;48:764–8.
38. Rippa M, Signorini M, Dallocchio F. A multiple role for the coenzyme in the mechanism of action of 6-phosphogluconate dehydrogenase: the oxidative decarboxylation of 2-deoxy-6-phosphogluconate. J Biol Chem. 1973;248:4920–5.
39. Zhang Y, Xu Y, Lu W, Li J, Yu S, Brown EJ, et al. G6PD-mediated increase in de novo NADP+ biosynthesis promotes antioxidant defense and tumor metastasis. Sci Adv. 2022;8:eabo0404.
40. Chen C, Lai X, Zhang Y, Xie L, Yu Z, Dan S, et al. NADPH metabolism determines the leukemogenic capacity and drug resistance of AML cells. Cell Rep. 2022;39:110650.
41. Ilter D, Drapela S, Schild T, Ward NP, Adhikari E, Low V, et al. NADK-mediated de novo NADP(H) synthesis is a metabolic adaptation essential for breast cancer metastasis. Redox Biol. 2023;61:102627.
42. Shao C, Lu W, Du Y, Yan W, Bao Q, Tian Y, et al. Cytosolic ME1 integrated with mitochondrial IDH2 supports tumor growth and metastasis. Redox Biol. 2020;36:101685.
43. Gillis JL, Hinneh JA, Ryan NK, Irani S, Moldovan M, Quek LE, et al. A feedback loop between the androgen receptor and 6-phosphogluconate dehydrogenase (6PGD) drives prostate cancer growth. eLife. 2021;10:e62586.
44. Petzold G, Fischer ES, Thomä NH. Structural basis of lenalidomide-induced CK1α degradation by the CRL4CRBN ubiquitin ligase. Nature. 2016;532:127–30.
45. Crowell PD, Giafaglione JM, Jones AE, Nunley NM, Hashimoto T, Delcourt AM, et al. MYC is a regulator of androgen receptor inhibition-induced metabolic requirements in prostate cancer. Cell Rep. 2023;42:113221.
46. Massie CE, Lynch A, Ramos-Montoya A, Boren J, Stark R, Fazli L, et al. The androgen receptor fuels prostate cancer by regulating central metabolism and biosynthesis. EMBO J. 2011;30:2719–33.
47. Yang SJ, Jeon SJ, Van Nguyen T, Deshaies RJ, Park CS, Lee KM. Ubiquitin-dependent proteasomal degradation of AMPK gamma subunit by Cereblon inhibits AMPK activity. Biochimica et Biophysica Acta (BBA)-Mol Cell Res. 2020;1867:118729.
48. Yang SJ, Jeon S, Baek JW, Lee KM, Park CS. Regulation of AMPK activity by CRBN is independent of the thalidomide-CRL4CRBN protein degradation axis. Pharmaceuticals. 2021;14:512.
49. Moon H, Min C, Kim G, Kim D, Kim K, Lee SA, et al. Crbn modulates calcium influx by regulating Orai1 during efferocytosis. Nat Commun. 2020;11:5489.

ACKNOWLEDGEMENTS

This work was supported by grants from the National Research Foundation of Korea (2017R1D1AB03028590 and RS-2023-00252326), and supported in part by a grant of the Korea Health Technology R&D Project through the Korea Health Industry Development Institute (KHIDI), funded by the Ministry of Health & Welfare, Republic of Korea (RS-2024-00512909). We acknowledge the gracious support of the GIST Research funds (GRI IIBR grant and Future-Leading Specialized Research Project, 2025). And, we thank Seunghee Ryu (GEM Biosciences), Saravanan Parameswaran, and Ellis I. Lee for their assistance and support.

AUTHOR CONTRIBUTIONS

KG, H-SY, and SKC conceptualized the study. KG, H-SY, H-SA, SS, and HSN performed the experiments and analyzed the data. JYH, SP, E-KK, J-YH, DYC, DP, C-SP, and S-GY provided essential study materials and reagents. KG, H-SY, and H-SA performed the statistical analyses. FDY-R, SMO, and MAM carried out binding energy calculations, molecular docking, and molecular dynamics simulations. KG, H-SY, and SKC drafted, reviewed, and edited the manuscript. SKC acquired funding and supervised the study.

COMPETING INTERESTS

The authors declare no competing interests.

ETHICS DECLARATION

Animal experiments in this study were approved by the Institutional Animal Care and Use Committee of Asan Institute for Life Sciences (Approval number 2020-13-195) and Inha University, Korea.

CONSENT FOR PUBLICATION

All authors approved for the publication.

ADDITIONAL INFORMATION

Supplementary information The online version contains supplementary material available at https://doi.org/10.1038/s41388-026-03717-9.

Correspondence and requests for materials should be addressed to Steve K. Cho.

Reprints and permission information is available at http://www.nature.com/reprints

Publisher's note Springer Nature remains neutral with regard to jurisdictional claims in published maps and institutional affiliations.